Silicon photonics temperature and refractive index sensor for curing process monitoring in composite material industry

Ioannis Poulopoulos, Charalampos Zervos, Georgios Syriopoulos, Jeroen Missinne, Michal Szaj, et al.

Ioannis Poulopoulos, Charalampos Zervos, Georgios Syriopoulos, Jeroen Missinne, Michal Szaj, Hercules Avramopoulos, "Silicon photonics temperature and refractive index sensor for curing process monitoring in composite material industry," Proc. SPIE 12139, Optical Sensing and Detection VII, 1213909 (17 May 2022); doi: 10.1117/12.2621285

SPIE.

Event: SPIE Photonics Europe, 2022, Strasbourg, France

Silicon photonics temperature and refractive index sensor for curing process monitoring in composite material industry

Giannis Poulopoulos[a], Charalampos Zervos[a], George Syriopoulos[a], Jeroen Missinne[b], Michal Szaj[c], Hercules Avramopoulos[a]
[a]Photonics Communications Research Laboratory National Technical University of Athens, Greece;
[b]Center for Microsystem Technology (CMST) Ghent University and imec Ghent, Belgium;
[c]Argotech a.s. Trutnov, Czech Republic;

ABSTRACT

Composite materials offer significant performance advantages due to their lightweight, high-strength, and high stiffness. This led to their adoption in several industrial sectors with particular emphasis on the aerospace industry which has undergone a transformation towards a composite-dominated new standard. In order to respond to the increased demand, it is mandatory to focus on an efficient and well-controlled curing cycle of the resin, which will lead to a significant reduction of cost and an increase in production speed. We investigate, a photonic solution, able of measure key monitoring values that facilitate optimization of the curing process.
Simulation and evaluation results on a bragg grating based photonic integrated sensor, developed in 220 nm Silicon-on-Insulator platform, are presented. A multi-sensor deployment is considered, enabling monitoring of the temperature and the refractive index of the resin. Serially coupled bragg grating photonic elements will enable concurrent monitoring of both temperature and refractive index. Several bragg configurations have been investigated and experimentally evaluated, specifically regular and phase-shifted ones. Both TE and TM polarization operation sensors that have been designed and fabricated, will be presented. Their sensitivity on resin temperature and refractive index variation will be discussed, resulting in a comparative study outlining the benefits and disadvantages of each solution. Refractive index sensors are realized by employing post-processing etching techniques on Multi-Project-Wafer run fabricated silicon chips, on top of the periodic bragg grating element. The comparative study takes into consideration TE and TM polarization operation, regular and phase-shifted bragg grating configuration elements, while evaluating their sensitivity in temperature and refractive index variations. Temperatures considered are in the range of 27 °C to 200 °C, while refractive index values lay between 1.5 and 1.6. A Figure-of-Merit is proposed to facilitate the selection of multi-sensor deployment for specific temperature and refractive index ranges.

Keywords: Photonic temperature sensor, composite material fabrication, Bragg grating, wide dynamic temperature range, miniaturized multi sensor, composite molds, silicon photonics,

1. INTRODUCTION

The performance advantages offered by composites over traditional materials, specifically lightweight, high strength, and high stiffness, has led to their growing adoption in several industrial sectors. They are ideal materials for those applications requiring highly advanced technologies, such as aircraft and automotive parts [1], but also for construction and infrastructure elements. The aerospace industry has undergone a transformation from a metal-driven world to a composite-dominated new standard [2], while the automotive industry has also been increasingly using composites for their cost and weight reduction and recyclability advantages [3]. The major drivers for growth in the composite market are represented by the increasing demand for lightweight materials in the aerospace and automotive industries [4]. To cater to the increase in this demand two considerations must be focused on in the composite industry, a) The efficient and controlled curing cycles to reduce costs and speed up production and b) the adoption of composite tools (molds) for their lower (10x less than metal tools), ease of movement, ease of construction, and lower price, compared to standard metal tools [5]. The sensor concept which is presented facilitates both abovementioned considerations. Optimization of the filling and curing cycles and, thus, increase productivity, by applying process monitoring techniques. Currently, manufacturers either insert fiber sensors inside the finished part [6],[7], which is not highly desirable since it compromises the mechanical properties of the part, or they use filling and curing cycles with high safety margins monitored via tool-embedded thermocouples and dielectric sensors [8]. However, the latter electric solutions suffer in terms of operating capabilities and the facilitation of

Optical Sensing and Detection VII, edited by Francis Berghmans, Ioanna Zergioti, Proc. of SPIE
Vol. 12139, 1213909 · © 2022 SPIE · 0277-786X · doi: 10.1117/12.2621285

integrating them in composite materials (due to their size and electrically conductive aspect when using carbon fibres). Photonic structures developed [9],[10], would be able to measure key monitoring values that facilitate optimisation of the curing process, while capitalizing on the silicon chip miniaturization and its robustness against electric and magnetic interference.

In this manuscript, simulation and evaluation results on a bragg grating based photonic integrated sensor, developed in 220 nm Silicon-on-Insulator platform, are presented. A multi-sensor deployment is considered, enabling monitoring of the temperature and the refractive index of the resin. Serially coupled bragg grating photonic elements will enable concurrent monitoring of both temperature and refractive index, by precisely designing reflection resonance wavelength of each element, through the specification of bragg grating pitch value. Both TE and TM polarization operation sensors that have been designed and fabricated, are presented. Their sensitivity on resin temperature and refractive index variation is discussed, resulting in a comparative study outlining the benefits and disadvantages of each solution. Temperatures considered are in the range of 27 °C to 200 °C, with a thermo-optic efficiency of 0.084 nm/°C, while refractive index values lay between 1.5 and 1.6.

In this paper, in Section 2 the concept of the photonic multi sensor will be presented as well as how it designed to be integrated into composite tools. In Section 3 the design considerations and methodology of a Bragg based Temperature and Refractive Index sensors are presented along with simulation results. Finally in Section 4 the testbed for Temperature sensor evaluation is presented using an interrogator commonly used in the composite industry for Fiber Bragg sensors as well as measurements showing a significant thermo-optic efficiency of 0.084 nm/°C across a dynamic range of 27 °C to 200 °C.

2. CONCEPT OF SENSOR

Composite parts manufacturing cycles depend significantly on tool heating and cooling rates and a controlled process will result in increased production and quality of composite materials. The presented sensors will achieve this by appropriate cure and flow monitoring of material parameters through the development of self-monitoring composite tool for resin transfer molding (RTM) infusion processes. Specifically for the sensor, a multi-sensor Photonic Integrated Circuit (PIC) is embedded in a composite tool using Through Thickness Reinforcement (TTR) techniques, employing Bragg based sensor design. The PIC is situated on the top of the sensor module and it comes into contact with the manufactured composite part. This allows the photonic sensor to measure Refractive Index (RI) through changes in the evanescent field of a Bragg sensing element. This setup is using only one fiber to couple the light in and out and it requires access to the PIC from the bottom side. A conceptual layout of the Bragg based sensors on a single PIC is shown in Figure 1 from the Top, while a cross-sectional view of the PIC shows the concept of realizing a T sensor and an RI sensor with exposure to the resin.

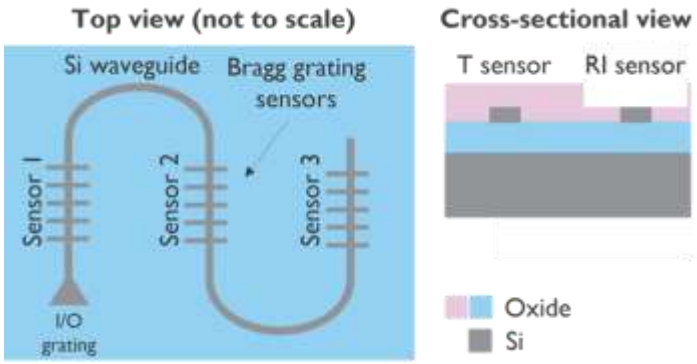

Figure 1. Top View of multi-sensor, in series configuration, with an Input/Output grating coupler. Each Bragg sensor is designed so that the reflected wavelength is different to allow all of them to be multiplexed in a single PIC. In the Cross-sectional view on the right, the RI sensor is exposed to the resin on the top by etching the top oxide layer.

The photonic sensor is designed to have a dynamic range, resolution and accuracy based on requirements of the Resin Transfer Molding (RTM) process for manufacturing composite parts. For the temperature sensor these values are displayed in Figure 2.

Parameter	Dynamic Range	Resolution
Temperature	Ambient – 200 °C	0.1 °C
Refractive Index	1.5 – 1.6	0.01

Figure 2. Table showing the Dynamic Range, and Resolution targets for Temperature (T) and Refractive Index (RI), based on the requirements of the Resin Transfer Molding (RTM) fabrication process for composite materials

The rate of change that is required is based on the application of the composite part that will be manufactured. For our purposes in aerospace, where quality control of the process is the priority, the fabrication of composite parts has typical single cycle duration in the order of a few hours. This is well within the speed that the photonic sensor acquires data considering the sampling rate lies at the kHz level. This fact makes the photonic sensors suitable for automotive applications as well which that has duration cycles in the order of minutes. In this paper and in the following sections the focus is on the design and testing of the temperature and refractive index sensors.

3. SENSORS DESIGN

In this section, the design methodology of Bragg grating structures, as well as their performance on temperature sensing operation, are presented. Bragg grating is a photonic element characterized by periodic modulation of refractive index (RI), across propagation direction, while at each refraction change, a small amount of light of certain wavelength is reflected. All the reflected light signals combine coherently to one large reflection at a particular wavelength at element's input. This is referred to as the Bragg condition, and the wavelength at which this reflection occurs is called the Bragg resonance wavelength. Bragg grating structures are designed for 220 nm Silicon On Insulator (SOI) technology. The design parameters that can be modified are the pitch (period) of the grating (Λ), corrugation width (*dw*), Filling Factor *(FF*), and effective index of propagation mode (n_{eff}). In our study only Bragg grating structures with *FF* value equal to 50% will be investigated. The resonance wavelength value (reflected wavelength) can be calculated via Bragg equation:

$$\lambda_{res} = 2 \cdot n_{eff} \cdot \Lambda$$

A schematic of a 50% FF Bragg grating structure, as well as its design parameters, is shown in Figure 3.

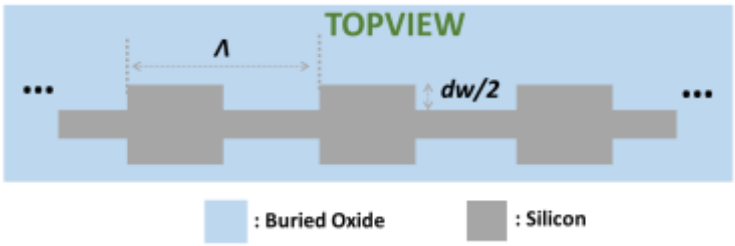

Figure 3. Top view of Bragg grating photonic element

The electromagnetic simulation software for mode calculations and propagation simulations used, is the commercially available Ansys Lumerical MODE Solutions [11]. The 220 nm top SOI platform supports both TE and TM polarization mode, whereas the nominal waveguide width is 450 nm and 500 nm for TE and TM polarization, respectively. The refractive index values for the layerstack materials are 3.47 for silicon waveguide, 1.45 for Buried Oxide layer, and 1.41 for cladding layer.

By appropriately choosing values for the aforementioned parameters, spectral response of the Bragg grating element can be calculated. EigenMode Expansion (EME) propagation solver was employed to calculate the reflection spectral response of a TE Bragg grating structure characterized by 320 nm pitch, 10 nm corrugation width, and 200 number of periods. Spectral response of this Bragg grating is plotted versus wavelength as the black line of the leftmost graph of Figure 4. As can be shown in Figure 4, by varying design parameters of the Bragg grating structure, specific changes of the spectral response occur, and more specifically:

- Varying grating pitch (Λ) → resonance wavelength is shifted

- Varying corrugation width (dw) → spectral bandwidth changes
- Varying Number of periods (N) → insertion loss value changes

To this end, a certain set of design parameters value is chosen, to comply with the specific requirements on wavelength shift, loss, and bandwidth of each use case requirements.

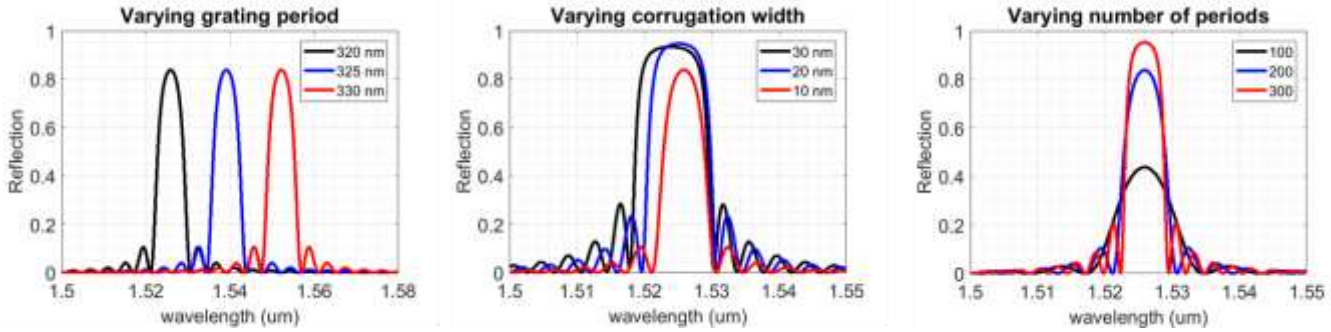

Figure 4 Effect on spectral response, varying Bragg grating design parameters

More specifically, in Figure 5 a set of reflection spectra can be shown for TE polarization operation Bragg grating structures, as calculated employing EME propagation solver for 220 nm top SOI waveguides and 450 nm nominal width. The effective index value as calculated for 450 nm width waveguides was calculated to be 2.3517. As can be seen in Figure 5(a), (c), and (d) the resonance wavelength is calculated to be 1532 nm, a result of the 324 nm period of Bragg gratings. By varying the corrugation width parameter of each Bragg grating, the 3-dB bandwidth is broadening with increasing the dw value (corrugation width). In Figure 5(b) the reflection spectrum of a Bragg grating with period value of 330 nm is shown, red shifted compared to the 324 nm period Bragg grating structures.

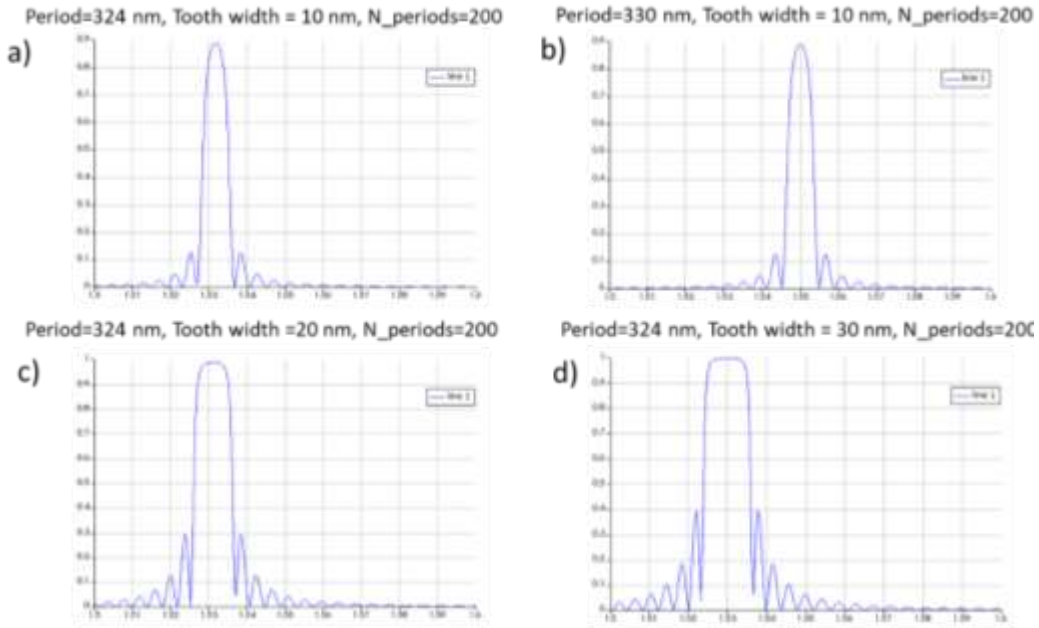

Figure 5. Calculated reflection spectrum for a series of TE polarization mode operation Bragg grating structures

In Figure 6, a set of reflection spectra can be seen for TM polarization operation Bragg grating structures, as calculated employing EME propagation solver for 220 nm top SOI waveguides and 500 nm nominal width. The effective index value for 450 nm width waveguides was calculated to be 1.6975. All the graphs in Figure 6 correspond to calculated reflection spectra for a series of Bragg grating components with a period of 438 nm. Tooth width value of each Bragg grating structure varies from 30 nm to 80 nm, whereas the higher this value is, the broader the reflection spectrum. It is important to also

note that the value of the tooth width affects the peak power of the reflected spectrum as well. As seen below, for the lowest value of tooth width (30 nm) the peak power of the reflection spectrum is low enough (43% - Figure 6(a)), compared to the 50 nm tooth width Bragg grating structure characterised by peak reflection power of 72% Figure 6(b), and to the 80 nm tooth width Bragg grating structure characterised by peak reflection power of 97% (Figure 6(c)).

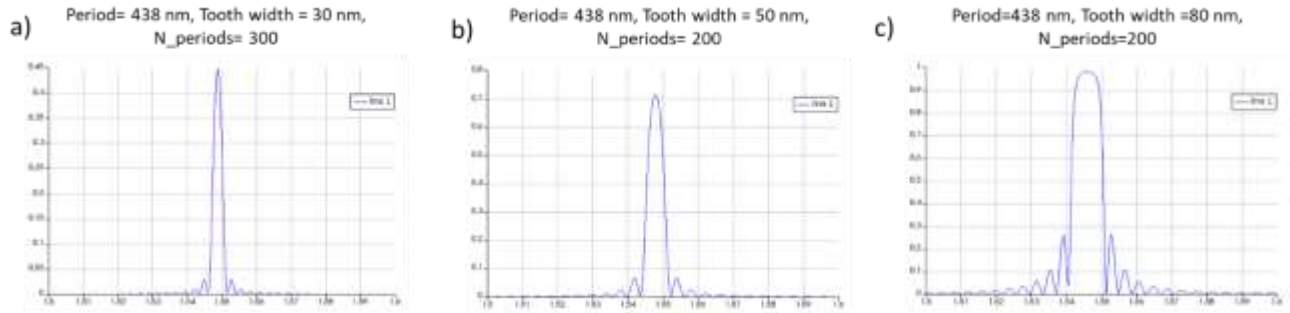

Figure 6- Calculated reflection spectrum for a series of TM polarization mode operation Bragg grating structures

Next, we discuss the results regarding phase-shifted Bragg grating structure. It is a Bragg grating, whereby a phase-shift is introduced between two identical gratings. The reflection spectrum of such a component is theoretically a narrow Lorentzian shape dip, in the middle of the grating spectrum. Apart from this dip in the spectrum, the specifications are almost the same as for the 'regular' Bragg gratings discussed above. A set of EME simulations for first order phase-shifted Bragg gratings was carried out.

Figure 7 shows the simulated reflection spectra for a series of TE polarization mode operation phase-shifted Bragg grating structures characterised by 20 nm corrugation width, 200 periods in length, and pitch of (a) 324 nm, (b) 326 nm, and (c) 328 nm. As can be observed, there is a very narrow dip in the middle of the Bragg grating spectrum, enabling accurate measurement of the central resonance wavelength. Increase in the pitch value results in a wavelength red-shift according to Bragg grating equation.

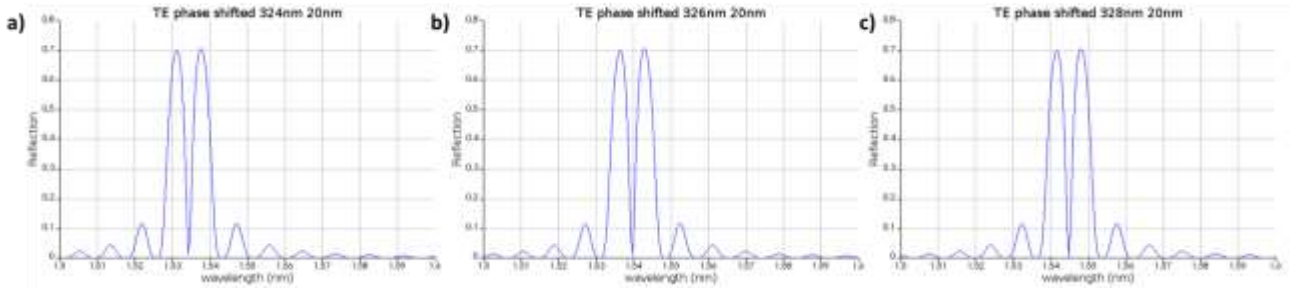

Figure 7- Calculated reflection spectrum for a series of TE polarization mode operation phase-shifted Bragg grating structures varying pitch value

Figure 8 shows the simulated reflection spectrum for a series of TE polarization mode operation phase-shifted Bragg grating structures characterised by pitch value of 328 nm, 200 periods in length, and corrugation width of (a) 20 nm, (b) 30 nm, and (c) 40 nm. This set of simulations was carried out to investigate the effect of corrugation width on the reflection spectrum of phase-shifted Bragg grating structures. As can be seen, increasing corrugation width results in increasing Bragg grating bandwidth (of the envelope transfer function – ignoring the phase-shift induced dip), i.e. the envelope 3-dB bandwidth as calculated from maxima was found to be (a)11.5nm, (b) 13.7 nm, and (c) 15.8 nm, for the different corrugation widths respectively. Along with the bandwidth increase, a reduction of insertion losses (i.e. increase in peak reflectivity) can be observed leading to a trade balance between losses and narrowband operation. To this end, given a certain number of Bragg gratings cover the entire area of C-band, a choice on the Bragg envelope bandwidth, and insertion losses, should be done to achieve low losses and no overlap between Bragg gratings, especially for this case where phase-shifted Braggs are employed for both sensing elements.

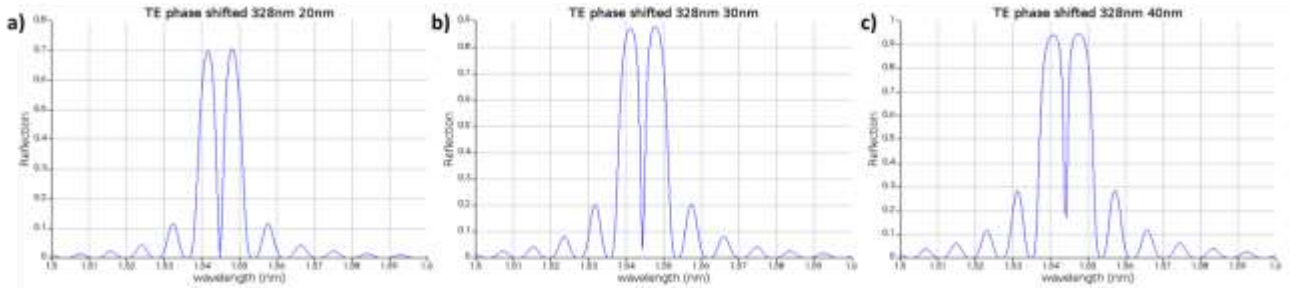

Figure 8- Calculated reflection spectrum for a series of TE polarization mode operation pi/2 phase-shifted Bragg grating structures varying corrugation width

After completing the Bragg grating element design, the thermo-optic response of these structures will be simulated. Temperature sensor is primarily based on thermo-optic effect, thus meaning exploiting the refractive index of silicon material by changing temperature. Thermo-optic coefficient of silicon is $\frac{dn}{dT} = 18 \times 10^{-5}\ K^{-1}$ for wavelength values around 1.55 μm. Thermal sensitivity can be analytically calculated via the following equation for Bragg gratings:

$$\frac{d\lambda}{dT} = \frac{\lambda}{n_g}\frac{dn_{eff}}{dn}\frac{dn}{dT}$$

However, instead of simulating the $\frac{dn_{eff}}{dn}$ fraction, to calculate thermal sensitivity, we carry out a set of thermal simulations to specify thermal sensitivity directly. Thermo-optical simulations were carried out in Mode Solutions Lumerical software for temperature range between 27 °C to 187 °C. The cross section of the silicon thermo-optic sensor is shown in Figure 9(a). Simulation results for a nominal TE polarization Bragg grating are shown in Figure 9(b), revealing the red-shift of resonance wavelength by increasing temperature.

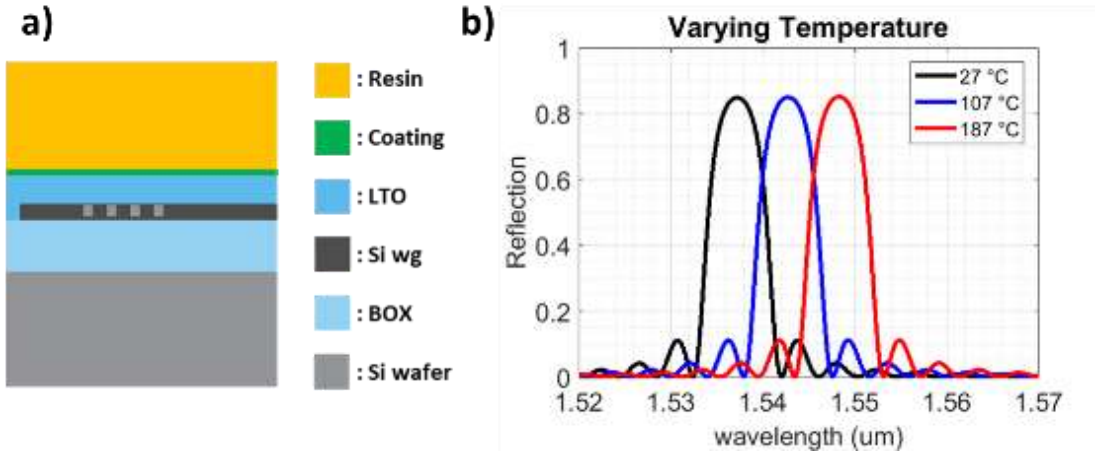

Figure 9.(a) Thermo-optic sensor cross section, and (b) Spectral response varying Temperature

A full set of thermo-optic simulations was then carried out for both TE and TM polarization mode. Wavelength shift is linear as shown in Figure 10, whereas the total wavelength shift (Temperature: 27 °C to 187 °C) is depicted for TE (blue line) and TM (red line) polarization operation. Thermo-optic wavelength tuning efficiency is simulated to be 0.070 nm/°C and 0.044 nm/°C for TE and TM polarization mode.

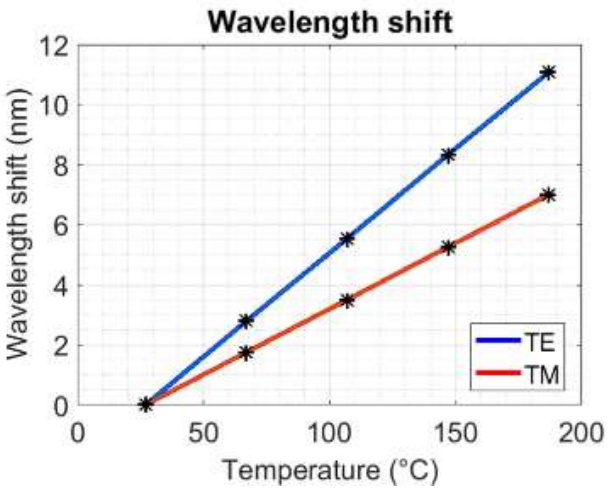

Figure 10. Wavelength shift varying temperature for TE and TM polarization operation

Temperature sensors will be used as reference sensors to calibrate RI and pressure sensors. To this end, temperature sensor should be insensitive to variations of RI value change. Regarding sensitivity of temperature sensor on resin RI change, a set of EME simulations was carried out to specify the wavelength shift of Bragg grating resonance wavelength by varying resin RI from a minimum (1.5) to maximum (1.6) expected value, co-varying the thickness and RI of coating material. Simulation results for TM polarization operation are shown in Figure 11(a) and indicate a small sensitivity of thermal sensor to resin RI change for coating height higher than 400 nm, independently of coating RI value. As shown in Figure 11(b), TE polarization operation Bragg grating is negligible independently of coating layer thickness and RI (wavelength shift values ~10^{-3}).

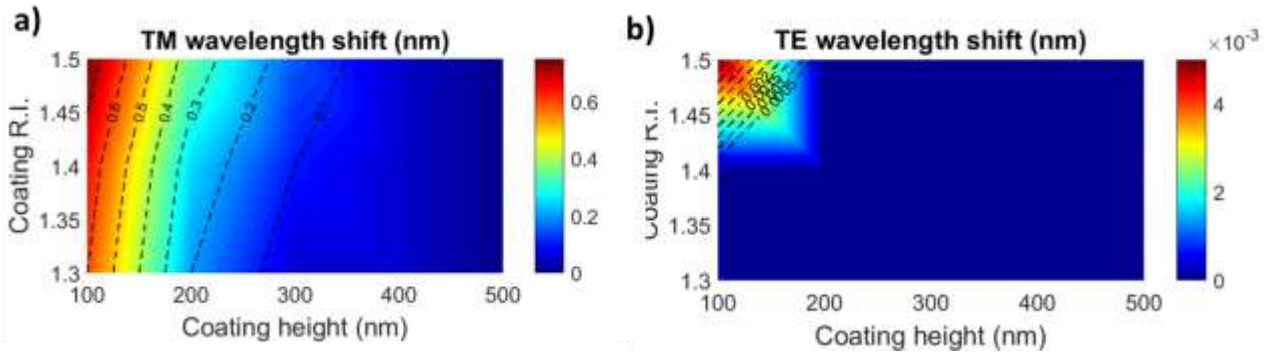

Figure 11. Temperature sensor sensitivity on resin RI change, varying coating thickness height and RI

Principle of operation of the RI sensor, is the change of the effective index of the propagating Bragg grating mode. This can be achieved, by enabling fraction of power of the propagating mode to be waveguided in the resin material. To enhance this effect, the LTO layer is etched after fabrication and the coating is deposited. As a result, the coating layer is the only one layer separating silicon waveguide and resin material. The layerstack described is shown in Figure 12(a). Simulation results are carried out in Lumerical Mode solutions simulation platform. In Figure 12(b), simulation results on wavelength shift for a nominal TM polarization operation Bragg grating RI sensor are depicted varying resin RI value from 1.5 to 1.6, calculating resonance wavelength shift of 0.020 nm/0.001 RIU.

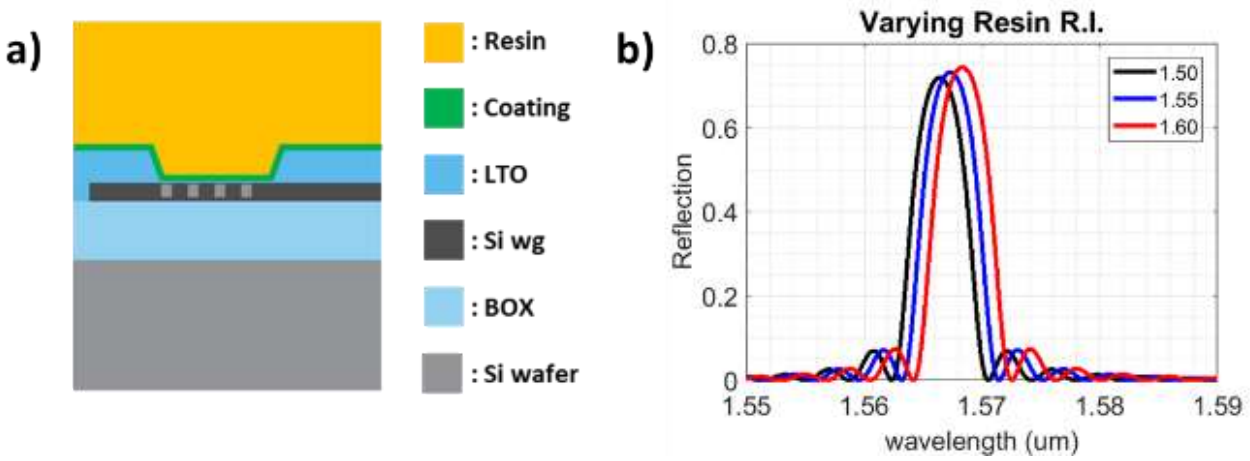

Figure 12 - (a) RI profile of RI sensor, and (b) wavelength shift varying resin RI

In Figure 13, simulation results on wavelength shift values varying resin RI from minimum to maximum (1.5 to 1.6) are depicted in logarithmic scale. Wavelength shift results are shown versus coating thickness (nm), varying coating RI from 1.3 to 1.5 with a step of 0.1. To note that given 1 pm measurement sensitivity of interrogator, wavelength shift value more than 0.1 nm is required. To this end, TE polarization operation can be feasible to detect resin RI change, only for coating layer thickness less than 200 nm. TM polarization Bragg grating is more sensitive to resin RI changes. As may be seen, wavelength shift is far higher than the wavelength shift limit of 0.1 nm, enabling realization of RI sensors independently of coating layer thickness and RI.

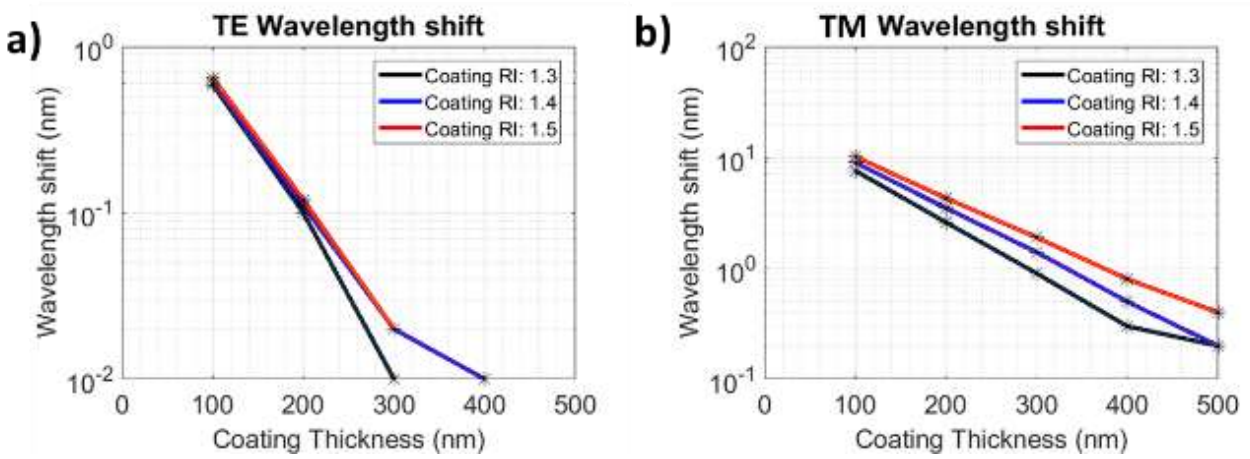

Figure 13 - Wavelength shift varying resin RI (1.5 to 1.6), versus coating layer thickness and RI

In order to characterize the performance of a temperature and RI sensor, the following Figure of Merit is proposed for a certain temperature at 160 °C, according to RTM requirements:

$$FOM = \frac{Temperature\ sensor\ sensitivity_T \cdot RI\ sensor\ sensitivity_{RI}}{Temperature\ sensor\ sensitivity_{RI}}$$

Where, $Temperature\ sensor\ sensitivity_T$ is the temperature sensor wavelength shift varying temperature, $Temperature\ sensor\ sensitivity_{RI}$ is the temperature sensor wavelength shift varying resin RI, and $RI\ sensor\ sensitivity_{RI}$ the RI sensor wavelength shift varying resin RI.

4. TESTBED AND RESULTS

In this paragraph the testbed to evaluate temperature sensing elements and the experimental results are discussed. As may be seen in Figure 14, a narrowband tunable laser is employed as light source provided by the FAZT I4G commercial interrogator. The interrogator covers 39.2 nm of C-band with a frequency of 2 kHz (1529 nm – 1568.2 nm). It operates on TE or TM polarization mode and for each wavelength it transmits, it measures the reflection optical power. The interrogator displays the whole spectrum, and it allows us to measure the exact resonance wavelength as well as the spectral characteristics of the Bragg grating reflection spectrum. The interrogator cannot be used to measure the exact power level of the reflection spectrum but only provides relative measurements. However, this is not critical for the evaluation measurements of the sensors which relies on the shift of the reflection resonance wavelength of the Bragg grating as the chip temperature varies.

As can be seen in Figure 14, an in-line fiber polarization controller (PC1) together with an in-line fiber polarizer, are used after the interrogator to align the interrogator output state of polarization with the 45° angle polarizer optical axis. By employing this configuration it is ensured that only a single state of polarization is transmitted after polarizer. A second in-line fiber polarization controller (PC2) is then employed, to select the state of polarization at the fiber tip, just before entering the chip under test. The reflection then follows the opposite direction, starting from PC2, passing through polarizer and PC1, and reaching the interrogator to be monitored. Also, a through port power meter is employed, to facilitate the alignment of the fibers on top of chip under test. All fibers used across the testbed setup are SMF.

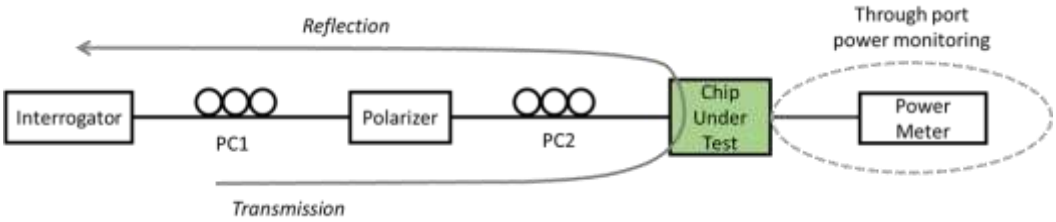

Figure 14. Testbed setup to measure reflection spectrum employing a FAZT I4G commercial interrogator

The testbed on which the chip is located, consists of 6-axis electrically controlled piezoelectric positioners, for the input and output fibers. The chip is located on a copper vacuum chuck to hold it firmly in place, which is embedded in the plated copper heater block. Fiber-to-chip alignment is enabled via optical inspection, using a camera on top of the chip, as well as via power monitor at the through port as already described. The heater block (plated copper block) hosts the vacuum chuck, an ohmic resistance heater as well as a temperature monitoring component. More specifically, in this bench setup, a ceramic heater with maximum power load of 30 W is embedded on the heater block, enabling temperature increase of the entire block up to 300 °C, while provides long-lasting and consistent performance. Cooling process is controlled via a fan placed next to the heater block. Temperature is then monitored via two processes, namely: a) employing a thermistor (Semitec 104GT2) which is capable of sensing up to 300 °C hosted on the heater block, and b) using a commercial FLIR thermometer (FLIR TG56) able to provide calibrated temperature measurements with high accuracy. The control of the heater and fan, as well as the monitoring of the thermistor is achieved via employing open-source code.

Data on the reflection spectrum are acquired by the interrogator (at 4kHz), after both input and through port fibers are optimally aligned to silicon chip, and both polarization controllers aligned to minimize insertion losses and maximize fiber to chip coupling efficiency for TE polarization mode operation. The mean-values of a series of 10 reflection spectra is calculated from the acquired data. The mean-value helps to smooth out any data due to instantaneous vibrations of the chip and bench that the chip is placed, allowing a determination of the wavelength shift with easy, while still providing a rate of measurement at 400 Hz. Before thermal load is applied to the heater, and thus chip temperature is increased, the chip temperature was measured to be 25.2 °C. Then, the chip temperature is increased from 25.2 °C to 40 °C, up to a maximum of 200 °C. The results are plotted in Figure 15, where the reflection spectra for 30 nm corrugation width gratings, with 200 periods of 328 nm in length varying chip temperature, for TE polarization operation, is shown. By increasing the chip temperature, the reflection spectrum is red-shifted. As can be seen, even for chip temperature of 200 °C, the reflection peak is in the range of interrogator reading spectrum, and thus the monitoring for all temperatures up to 200 °C is feasible for the 328 nm pitch grating, with thermo-optic tuning efficiency of 0.0825 nm/°C. Difference of peak power levels after varying temperatures, even that as already mentioned the power levels can only be characterized as “relative”, could be explained due to thermal expansion of silicon structures when they are heated, thus contributing to fiber-to-chip misalignment, as well as narrowband input grating coupler structures operation.

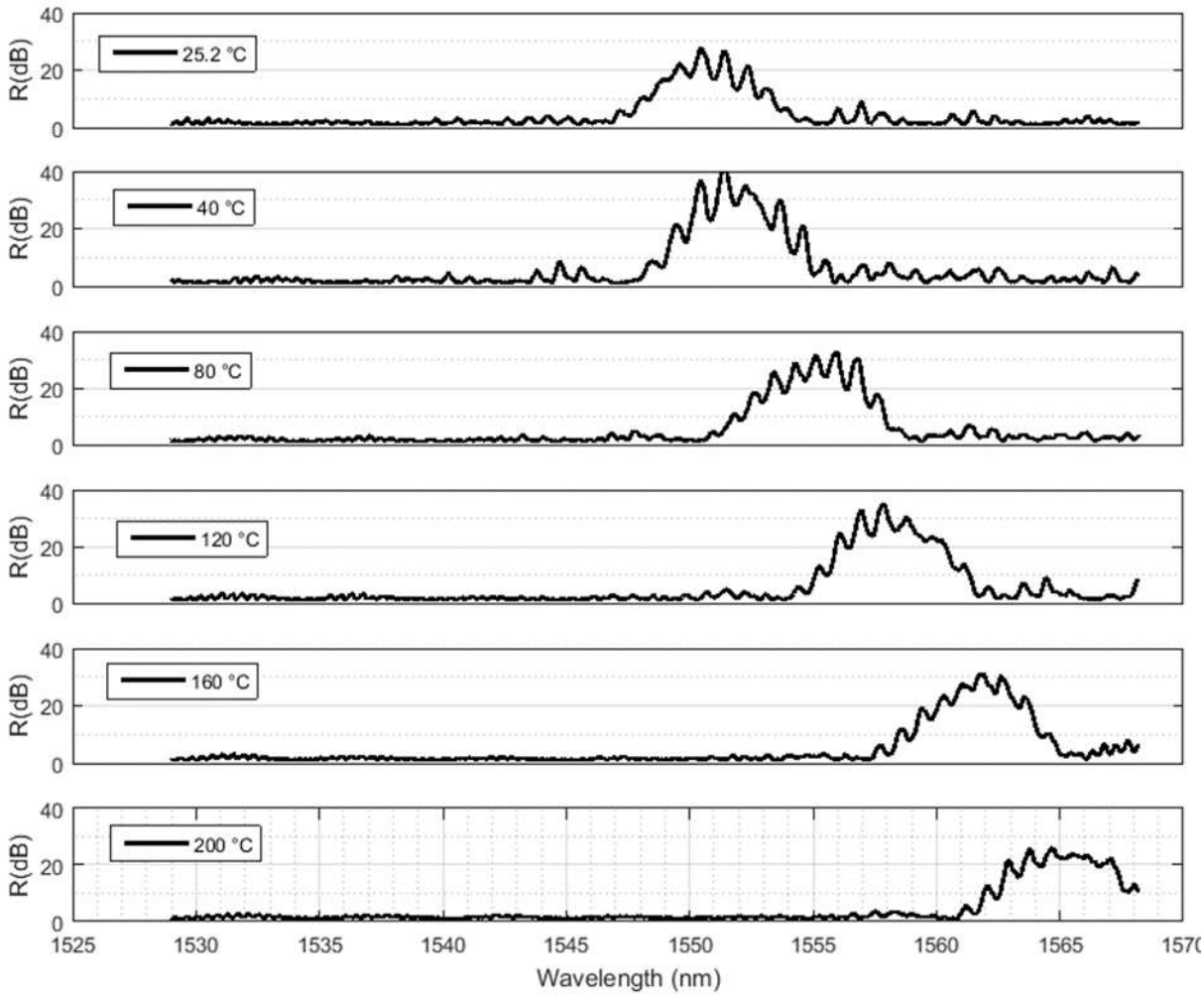

Figure 15. Reflection spectrum measurements varying chip temperature for TE bragg grating structure

The reflection spectrum is characterized by ripples which are due to reflections taking place at the fiber tip-to-grating coupler optical interface, and their effect can be minimized by employing phase matching liquid at this interface.
As may be seen in the linear regression line shown in Figure 16, a mean value of thermo-optic tuning efficiency of 0.0825 nm/°C is measured, characterized by high linearity ($R^2 = 0.99154$), while this value has the potential to be further enhanced by optimizing the fiber-to-grating coupler interface.

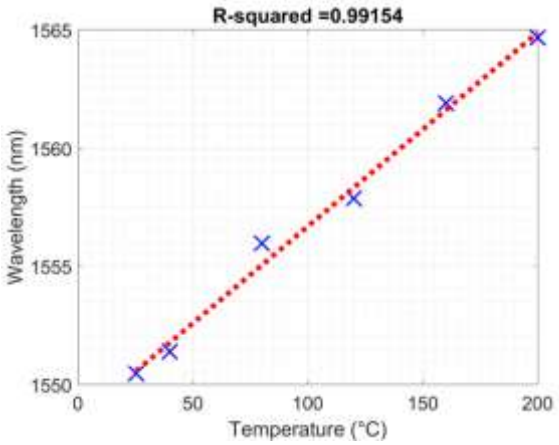

Figure 16. Resonance wavelength varying temperature, and its linear regression for TE bragg grating structure

The results regarding the phase-shifted TE polarization bragg grating, with design parameters of 324 nm pitch, tooth width of 20 nm, and number of periods = 200, are shown in Figure 17.

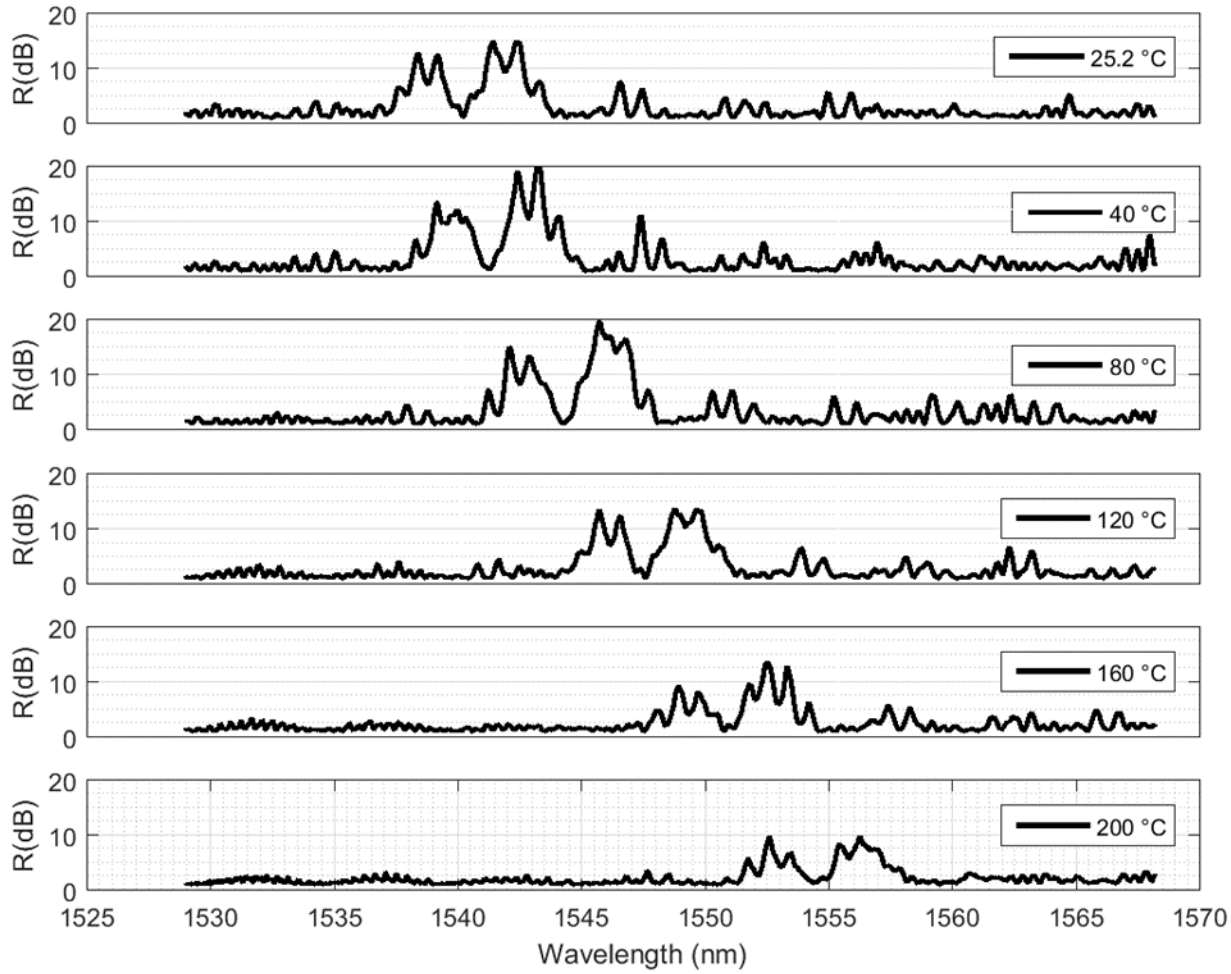

Figure 17. Reflection spectrum measurements varying chip temperature for phase-shifted TE bragg grating structure

As seen in Figure 18, a mean value of thermo-optic tuning efficiency of 0.0825 nm/°C is measured, characterized by high linearity (R^2 = 0.99967). It is clear that the dip at the reflection spectrum enables high accuracy on the temperature measurement, and thus an increased R^2 value.

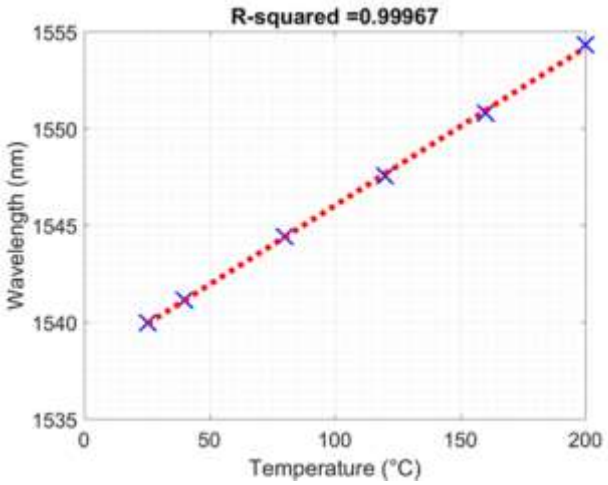

Figure 18. Resonance wavelength varying temperature, and its linear regression for TE phase-shifted bragg grating structure

5. CONCLUSIONS

We present the design and evaluation of a miniaturized novel photonic integrated sensor, capable of measuring key monitoring values that facilitate optimization of the curing process. Both regular and phase shifted bragg gratings are presented, and their sensitivity is discussed. Both TE and TM polarization operation sensors that have been designed and fabricated, are presented. Their sensitivity on resin temperature and refractive index variation is discussed, resulting in a comparative study outlining the benefits and disadvantages of each solution. Temperatures considered are in the range of 27 °C to 200 °C, with a thermo-optic efficiency of 0.084 nm/°C, while refractive index values lay between 1.5 and 1.6. TE polarization sensors show a better response to temperature variation, while TM polarization sensors, due to the low confinement of bragg grating mode in silicon core (stronger top-evanescent field outside of the silicon) are more suited for refractive index sensors (greater interaction of propagating mode field with resin), hence a Figure-of-Merit is proposed to facilitate the selection of multi-sensor deployment for specific temperature and refractive index ranges.

6. ACKNOWLEDGEMENTS

This work has received funding from the European Union's Horizon 2020 innovation programme under grant agreement No. 871875 (SEER).

REFERENCES

[1] https://www.ncbi.nlm.nih.gov/pmc/articles/PMC5796376/
[2] http://compositesmanufacturingmagazine.com/2018/01/2018-composites-manufacturing-state-of-the-industry-report/
[3] https://compositesuk.co.uk/composite-materials/applications/automotive
[4] https://www.prnewswire.com/news-releases/global-composites-industry-overview-2018-2023---increasing-demand-for-lightweight-materials-in-the-aerospace--defense-and-automotive-industry-300673139.html
[5] https://info.dte.co.uk/why-composite-materials-are-the-best-thing-for-the-automotive-sector
[6] Pierre Ferdinand, Sylvain Magne, Véronique Dewynter-Marty, Stéphane Rougeault, Laurent Maurin. Applications of Fiber Bragg Grating sensors in the composite industry. MRS Bulletin, Cambridge University Press (CUP), 2002, 27 (5), pp.400-407. ff10.1557/mrs2002.126ff. ffcea-01841910f

[7] G. Rajan et al., "Performance analysis and comparison of composite materials embedded with different optical fiber sensor types," SENSORS, 2011 IEEE, 2011, pp. 351-354, doi: 10.1109/ICSENS.2011.6127055.
[8] Tifkitsis, K. I., & Skordos, A. A. (2019). A novel dielectric sensor for process monitoring of carbon fibre composites manufacture. Composites Part A: Applied Science and Manufacturing, 123, 180-189.
[9] Haitan Xu, Mohammad Hafezi, J. Fan, J. M. Taylor, G. F. Strouse, and Zeeshan Ahmed, "Ultra-sensitive chip-based photonic temperature sensor using ring resonator structures," Opt. Express 22, 3098-3104 (2014)
[10] Li-Yuan Chiang, Chun-Ta Wang, Ting-Syuan Lin, Steve Pappert, and Paul Yu, "Highly sensitive silicon photonic temperature sensor based on liquid crystal filled slot waveguide directional coupler," Opt. Express 28, 29345-29356 (2020)
[11] https://www.lumerical.com/